

All-conjugated cationic copolythiophene “rod–rod” block copolyelectrolytes: synthesis, optical properties and solvent-dependent assembly†

Cite this: DOI: 10.1039/c4py00037d

Amandine Thomas,^{ab} Judith E. Houston,^c Niko Van den Brande,^d Julien De Winter,^e Michèle Chevrier,^{af} Richard K. Heenan,^g Ann E. Terry,^g Sébastien Richeter,^a Ahmad Mehdi,^a Bruno Van Mele,^d Philippe Dubois,^f Roberto Lazzaroni,^b Pascal Gerbaux,^e Rachel C. Evans^{*ch} and Sébastien Clément^{*a}

Amphiphilic diblock copolythiophenes were synthesised by an efficient two-step strategy. The diblock copolyelectrolytes were obtained *via* quasi-living Kumada catalyst-transfer polycondensation followed by quaternisation of the bromohexyl side chains of one of the monomer constituents into *N*-methylimidazolium, pyridinium, trimethylammonium or trimethylphosphonium units. The effect of the nature of the charged group on the thermal properties was investigated by Rapid Heat–Cool (RHC) calorimetry measurements. The solvent-driven assembly of these block copolyelectrolytes in chloroform (CHCl₃), water, methanol (MeOH), water–MeOH mixtures and in subsequently prepared thin films was investigated using a combination of photoluminescence, scattering and microscopic techniques. The rigid rod-structure of the block copolyelectrolytes led to the formation of core–shell cylindrical or disc-like aggregates in solution, with features determined by the nature of the solvent. AFM studies revealed that the aggregates formed in solution can be transferred into thin films allowing for the reliable control of the self-organisation process and the resulting nanoscale architecture.

Received 10th January 2014
Accepted 23rd January 2014

DOI: 10.1039/c4py00037d

www.rsc.org/polymers

^aInstitut Charles Gerhardt – UMR 5253, Equipe Chimie Moléculaire et Organisation du Solide, Université Montpellier 2 – CC1701, Place Eugène Bataillon, F-34095 Montpellier Cedex 05, France. E-mail: sebastien.clement02@univ-montp2.fr; Tel: +33 467143971

^bLaboratory for Chemistry of Novel Materials, Center for Innovation in Materials and Polymers, Research Institute for Science and Engineering of Materials, University of Mons – UMONS, 23 Place du Parc, B-7000 Mons, Belgium

^cSchool of Chemistry, The University of Dublin, Trinity College, Dublin 2, Ireland. E-mail: raevans@tcd.ie

^dPhysical Chemistry and Polymer Science (FYSC), Vrije Universiteit Brussel (VUB), Pleinlaan 2, B-1050 Brussels, Belgium

^eLaboratory of organic synthesis and mass spectrometry, Interdisciplinary Centre for Mass Spectrometry, University of Mons-UMONS, 23 Place du Parc, B-7000 Mons, Belgium

^fLaboratory for Polymeric and Composites Materials, Center for Innovation in Materials and Polymers, Research Institute for Science and Engineering of Materials, University of Mons – UMONS, 23 Place du Parc, B-7000 Mons, Belgium

^gISIS, STFC, Rutherford Appleton Laboratory, Didcot, Oxon OX11 0QX, UK

^hCentre for Research on Adaptive Nanostructures and Nanodevices (CRANN), Trinity College Dublin, Dublin 2, Ireland

† Electronic supplementary information (ESI) available: ¹H, ¹³C{¹H} NMR spectra of the precursor block copolymers and the ionic block copolythiophenes, ³¹P{¹H} NMR spectra of P3HT-*b*-P3HTPMe₃, MALDI-TOF spectra of P3HT-*b*-P3HTBr. UV/Vis spectra of P3HT-*b*-CPE. Absorption, excitation and PL spectra of P3HT-*b*-CPE in H₂O–MeOH mixtures. Correllogram and size distribution obtained by DLS of P3HT-*b*-P3HTPMe₃ in MeOH. SANS data analysis for P3HT-*b*-CPEs. AFM images of P3HT-*b*-CPEs drop-cast from MeOH, H₂O or H₂O/MeOH mixture. See DOI: 10.1039/c4py00037d

Introduction

Conjugated polyelectrolytes (CPEs) are defined as polymers with an extended π -conjugated backbone and ionic pendant groups, which combine the organic semiconductor properties and charge-mediated characteristics of polyelectrolytes in a single functional material.¹ As such, CPEs constitute a promising class of materials for application in optoelectronic devices, chemo- and biosensors, and biological imaging.² However, since device performance depends on both the optoelectronic properties and nanoscale morphology of the polymer (which are intrinsically linked), understanding the parameters and physical processes influencing the polymer morphology and its interdependent optoelectronic properties is of crucial importance.³

Recently, self-assembly strategies have emerged as an elegant approach for the design and fabrication of reproducible nanoscale aggregates from conjugated polyelectrolyte building blocks.⁴ For example, co-assembly with oppositely charged species in solution (*e.g.* ionic surfactants,⁵ metal ions⁶ and complexes/clusters,⁷ DNA⁸) is facilitated *via* electrostatic interactions with the charged side-chains, leading to the formation of extended networks exhibiting structural and morphological organisation across multiple length scales.

Block copolymers may also provide an alternative interesting route to control the self-assembly into nanostructured morphologies.⁹ However, the rod-like nature of most

conjugated polymers complicates the self-assembly of corresponding block copolymers through an interplay of nanophase separation and bulk crystallisation.^{9a} Nonetheless, self-organisation at the nanoscale into lamellar/fibrillar morphology can be obtained in all-conjugated rod-rod block copolymers.¹⁰ The self-assembly of such copolymers into stable nanostructures of different shapes or morphologies is dictated by both the chain stiffness and the solubility of the individual blocks.¹¹ In this respect, the combination of covalently bound ionic and neutral blocks can be used to introduce solubility gradients across the copolymer structure and subsequent self-assembly into organised nanostructures can be induced by solvent-mediation.¹²

Scherf *et al.* have in particular reported that all-conjugated cationic “rod-rod” block copolyelectrolytes containing two electronically different conjugated blocks (namely, polyfluorene and polythiophene blocks) exhibit solvent-mediated self-assembly in mixtures of selective and non-selective solvents, such as water-methanol (MeOH) and water-THF, which provides a convenient method of modulating the photoluminescence properties *via* segregation of the two blocks.^{12a-d} Control of the nanomorphology of the self-assembled aggregates (*e.g.* vesicles, rods, *etc.*) may be obtained through judicious selection of the concentration, solvent or molecular weight of the polymer.¹² Similar changes in nanophase morphology were also observed in all-conjugated cationic diblock copolymers composed of two polyfluorene blocks (a neutral block bound to a cationic block) in protic or non-protic solvents (MeOH *vs.* THF).¹³

Maes *et al.* have recently reported a family of ionic polythiophene-based homopolymers and random copolymers functionalised with imidazolium-terminated side chains at different monomer ratios.¹⁴ However, the analogous all-conjugated cationic diblock polythiophene copolymers have been scarcely studied.^{12e} This is somewhat surprising on two counts. Firstly, oligo- and polythiophenes are well-known to undergo temperature- and solvent-induced conformational changes which result in thermo- or solvato-chromatic responses in their optical properties (absorbance and fluorescence).¹⁵ Secondly, poly(3-hexylthiophene) (**P3HT**) is by far the most commonly used electron donor material in organic photovoltaics (OPV)¹⁶ and conjugated polyelectrolytes have also found application as interfacial layers in bulk heterojunction OPV devices.¹⁷ Significant efforts have been dedicated to the synthesis of sophisticated polythiophene derivatives, with the aim of improved morphological control and enhanced thermal stability.¹⁸ Amphiphilic diblock polythiophene copolymers are thus extremely attractive in this respect as they should afford concomitant tailoring of both the nanoscale morphology and the optical properties *via* solvent-induced self-assembly.

Control of the molecular weight and, in particular, the requirement for a narrow molecular weight distribution are also important parameters to be considered when designing new diblock copolymers for the purpose of self-assembly.^{9a-f} Moreover, the molecular weight of ionic polythiophenes has been identified as a crucial parameter influencing the performance of OPV devices.^{18a} In this respect, the Kumada Catalyst Transfer

Polycondensation (KCTP) method, which enables chain-growth polymerisation and leads to the synthesis of conjugated polymers with relatively high molecular weight, narrow polydispersity and minimised termination side reactions, is a tool of choice to obtain ordered nanostructures.¹⁹ This method has been successfully applied to the synthesis of well-defined polyfluorenes,²⁰ polypyrroles²¹ and polycarbazoles.²² Moreover, the “living” chain growth mechanism of the KCTP reaction might afford straightforward access to regioregular block copolymers through a one-pot procedure.^{19c,23}

Herein, we report on the synthesis of amphiphilic “rod-rod” block copolyelectrolytes composed of two polythiophene blocks (a neutral block bound to a cationic block) bearing either *N*-methylimidazolium, pyridinium, trimethylammonium or trimethylphosphonium groups prepared by using the KCTP method. The effects of the nature of the charged group on the optical and thermal properties are investigated. The aggregation properties of the CPEs in selective and non-selective solvent mixtures (H₂O-MeOH) are evaluated using a combination of dynamic light scattering (DLS), small-angle neutron scattering (SANS) and atomic force microscopy (AFM), with the goal of identifying key structure-property relationships in this novel class of materials.

Experimental

Materials and characterisation methods

All reactions were carried out under argon or nitrogen using standard high-vacuum and Schlenk techniques. 2-Bromo-3-hexyl-5-iodothiophene and 2,5-dibromo-3-bromohexylthiophene were prepared according to literature methods.^{10a,24} Dry THF was obtained by distilling over CaH₂, then Na-benzophenone. Dry toluene was obtained by distilling over Na. Chemicals were obtained from Alfa-Aesar, Sigma-Aldrich and Acros and used as received. All NMR spectra were acquired with a Bruker Avance 300 spectrometer (¹H 300.13 MHz, ¹³C{¹H} 75.48 MHz and ³¹P{¹H} 121.49 MHz) using the solvent as the chemical shift standard, except for ³¹P{¹H} NMR, where the chemical shifts are relative to 85% H₃PO₄ in D₂O. All chemical shifts and coupling constants are reported in ppm and Hz, respectively. Elemental analyses were performed with a ThermoFinnigan Flash EA 1112 instrument and expressed in terms of the weight percent ratio of nitrogen to sulphur atoms. Number-averaged (*M_n*), weight-averaged (*M_w*) molecular weights and the molecular weight distribution (PDI) of **P3HT-*b*-P3HTBr** were measured using size exclusion chromatography (SEC) on a Polymer Laboratories liquid chromatograph equipped with a PL-DG802 degasser, an isocratic HPLC pump LC 1120 (flow rate = 1 mL min⁻¹), a Marathon autosampler (loop volume = 200 μL, solution conc. = 1 mg mL⁻¹), a PL-DRI refractive index detector and three columns: a PL gel 10 μm guard column and two PL gel Mixed-B 10 μm columns (linear columns for separation of MWPS ranging from 500 to 10⁶ daltons). The eluent used was THF at a flow rate of 1 mL min⁻¹ at 40 °C. Polystyrene standards were used to calibrate the SEC. Matrix-assisted laser desorption/ionisation time-of-flight (MALDI-ToF) mass spectra were recorded using a Water QToF Premier mass

spectrometer equipped with a nitrogen laser, operating at 337 nm with a maximum output of 500 J m⁻² delivered to the sample in 4 ns pulses at 20 Hz repeating rate. Mass analyses were performed in reflection mode at a resolution of about 10 000. All samples were analysed using (DCTB) *trans*-2-[3-(4-*tert*-butylphenyl)-2-methylprop-2-enylidene]malononitrile. This matrix was prepared as a 40 mg mL⁻¹ solution in CHCl₃.²⁵ The matrix solution (1 μL) was applied to a stainless steel target and air dried. Polymer samples were dissolved in CHCl₃ to obtain 1 mg mL⁻¹ solutions. 1 μL aliquots of these solutions were applied onto the target area already bearing the matrix crystals and air dried. For the recording of the single-stage MS spectra, the quadrupole (rf-only mode) was set to pass ions from *m/z* 500 to *m/z* 15 000, and all ions were transmitted into the pusher region of the time-of-flight analyser where they were mass analysed with 1 s integration time. Rapid Heat-Cool (RHC) calorimetry experiments were performed on a prototype RHC from TA Instruments, equipped with liquid nitrogen cooling and specifically designed for operation at high scanning rates.^{26,27} RHC measurements were performed at 500 K min⁻¹ in aluminium non-hermetic crucibles, using neon (6 mL min⁻¹) as a purge gas. For comparison with block copolymers, pure CPE homopolymers were synthesised from a **P3HTBr** precursor (*M_n* = 14 900 g mol⁻¹, *M_w* = 20 700 g mol⁻¹, PDI = 1.39) following a recently reported procedure.⁸ UV/Vis absorption and fluorescence spectra were recorded at room temperature on a Shimadzu UV2401 PC UV/Vis scanning spectrometer and a Fluorolog-3 (Horiba Jobin Yvon) spectrophotometer, respectively. Emission and excitation spectra were corrected for the wavelength response of the system using correction factors supplied by the manufacturer. Fluorescence quantum yields (Φ_F) were measured using tetraphenylporphyrin (TPP) in toluene as a standard (Φ_F = 0.11).²⁸ Dynamic light scattering measurements were performed using a Zetasizer Nano series nano-ZS (Malvern Instruments, U.K.) in the back-scattering configuration (175°). Cumulant analysis of the correlation function was used to determine the mean hydrodynamic diameter (*Z*-average) and the polydispersity of each sample.²⁹ AFM measurements were performed using an Asylum Research MFP-3D™ instrument mounted on an anti-vibration plinth, in the tapping mode at room temperature under ambient conditions. The silicon cantilevers used were 125 μm in length and had a resonance frequency of ~150 kHz. All raw AFM images were visualised and analysed using the Gwyddion 2.31 software. SANS was carried out on a Sans2d small-angle diffractometer at the ISIS Pulsed Neutron Source (STFC Rutherford Appleton Laboratory, Didcot, U.K.).³⁰ A simultaneous *q*-range of ~0.004–0.6 Å⁻¹ was achieved utilising an incident wavelength range of 1.75–16.5 Å separated by time-of-flight and employing an instrument setup of *L*₁ = *L*₂ = 4 m, with the 1 m² detector offset vertically 150 mm and sideways 150 mm. $q = (4\pi/\lambda)\sin(\theta/2)$, where λ is the wavelength and θ is the scattering angle. Samples were prepared in deuterated solvents, to provide good neutron scattering contrast. Each raw scattering dataset was corrected for the detector efficiencies, sample transmission and background scattering and converted to scattering cross-section data ($\partial\Sigma/\partial\Omega$ vs. *q*) using the instrument-specific software.³¹ These

data were placed on an absolute scale (cm⁻¹) using the scattering from a standard sample (a solid blend of hydrogenated and perdeuterated polystyrene) in accordance with established procedures.³² The scattering functions were fit using non-linear least-squares analysis to a Core-Shell-Cylinder model using the SasView programme.³³ Full details of the models and the fitting procedure can be found in the ESI.†

Synthesis

Poly[3-hexylthiophene)-2,5-diyl]-block-poly[3-(6-bromohexyl)-thiophene-2,5-diyl] block copolymer (P3HT-*b*-P3HTBr). Two round-bottomed flasks (100 mL) were dried by heating under reduced pressure and cooled to room temperature. 2-Bromo-3-hexyl-5-iodothiophene (1.22 g, 3.3 mmol) was dried by three successive azeotropic distillations with toluene, and then dry THF (15 mL) was added. A 2 mol L⁻¹ solution of *i*-PrMgCl in THF (1.65 mL) was added *via* a syringe, and the mixture was stirred at 0 °C for 30 min (solution A). Solution A was added in one portion to the Ni(dppp)Cl₂ catalyst (59 mg) in THF (10 mL). In the other flask, 2.7 mmol of 2,5-dibromo-3-bromohexylthiophene (1.09 g), previously dried by azeotropic distillation, was reacted with *i*-PrMgCl (1.35 mL) in the same manner (solution B). After stirring the reaction mixture for 3 h, solution B was added to the previous mixture *via* a syringe, and the resulting solution was stirred overnight. The reaction was quenched quickly by pouring HCl aq. (5 M) into the solution and stirring for 0.5 h. Then, the mixture was precipitated in cold MeOH and filtered. The product was washed well with MeOH and hexane to afford a red solid, **P3HT-*b*-P3HTBr**. Yield: 0.99 g (82%). ¹H NMR (CDCl₃): δ = 0.90 (t, 3H, CH₃, ³*J*_{H-H} = 6.8 Hz), 1.62 (m, 16H, CH₂), 2.80 (t, 4H, CH₂-Th, ³*J*_{H-H} = 7.9 Hz), 3.42 (t, 2H, CH₂-Br, ³*J*_{H-H} = 6.7 Hz), 6.98 (s, 2H, Th) ppm. ¹³C{¹H} NMR (CDCl₃): 14.3, 22.8, 28.1, 28.8, 29.4, 29.6, 30.5, 30.7, 31.8, 32.9, 34.0, 128.8, 130.7, 130.8, 139.8, 140.0. UV/Vis (CHCl₃): λ_{\max} = 450 nm; SEC (THF, PS standards): *M_n* = 11 000 g mol⁻¹, *M_w* = 12 300 g mol⁻¹, PDI = 1.12.

General procedure for the synthesis of P3HT-*b*-P3HTIm and P3HT-*b*-P3HTPy block copolyelectrolytes. Block copolymer **P3HT-*b*-P3HTBr** (150 mg) was allowed to react with 1-methylimidazole (10 mL) or pyridine (10 mL) in refluxing CHCl₃ (10 mL) for 2 days. After cooling to room temperature, the mixture was poured into Et₂O to precipitate the polyelectrolytes **P3HT-*b*-P3HTIm** and **P3HT-*b*-P3HTPy**. The crude polymers obtained were repeatedly washed with diethyl ether to remove excess of 1-methylimidazole or pyridine, and then dried under vacuum at 40 °C. The solid polymers **P3HT-*b*-P3HTIm** and **P3HT-*b*-P3HTPy** were further purified in refluxing diethyl ether using a Soxhlet apparatus overnight and finally, dried under vacuum at 40 °C.

P3HT-*b*-P3HTIm. Yield: 80%, ¹H NMR (CDCl₃): δ = 0.89 (br.), 1.19–1.47 (br.), 1.69 (br.), 1.90 (br.), 2.78 (br.), 3.19 (br.), 4.05 (br.), 4.34 (br.), 6.97 (br.), 7.74 (br.), 9.92 (br.) ppm. ¹³C{¹H} NMR (CDCl₃): δ = 14.2, 22.8, 26.3, 29.1, 29.4, 29.6, 30.5, 30.6, 31.8, 36.9, 50.1, 122.8, 124.1, 128.7, 130.6, 133.8, 136.7, 140.0 ppm. UV/Vis (CHCl₃): λ_{\max} = 452 nm; anal. calcd: *N/S* 0.86, found 0.86.

P3HT-*b*-P3HTPy. Yield: 81%, ¹H NMR (CDCl₃): δ = 0.91 (br.), 1.27–1.50 (br.), 1.70 (br.), 2.04 (br.), 2.80 (br.), 4.00 (br.), 6.96

(br.), 8.16 (br.), 8.60 (br.), 9.50 (br.) ppm. $^{13}\text{C}\{^1\text{H}\}$ NMR (CDCl_3): $\delta = 15.4, 23.8, 27.1, 30.2, 30.5, 30.7, 31.7, 32.8, 33.2, 62.9, 129.8, 131.7, 134.9, 141.1, 146.3, 147.0$ ppm. UV/Vis (CHCl_3): $\lambda_{\text{max}} = 455$ nm; anal. calcd: N/S 0.43, found 0.41.

General procedure for the synthesis of P3HT-*b*-P3HTNMe₃ and P3HT-*b*-P3HTPMe₃ block copolyelectrolytes. Block copolymer P3HT-*b*-P3HTBr (150 mg) was introduced into a 100 mL two-necked flask equipped for stirring and dissolved in CHCl_3 (15 mL). 12 mL of a solution of trimethylamine or trimethylphosphine (1.0 M in THF) were added and the mixture was stirred at 40 °C for 48 h. After cooling to room temperature, the solvent mixture was evaporated and the residue was dissolved in the minimum amount of CHCl_3 and poured into Et_2O to precipitate the polyelectrolytes P3HT-*b*-P3HTNMe₃ or P3HT-*b*-P3HTPMe₃. The crude products obtained were repeatedly washed with diethyl ether and dried under vacuum at 40 °C. P3HT-*b*-P3HTNMe₃ and P3HT-*b*-P3HTPMe₃ were further purified with refluxing diethyl ether using a Soxhlet apparatus overnight and finally, dried under vacuum at 40 °C.

P3HT-*b*-P3HTNMe₃. Yield: 79%, ^1H NMR (CDCl_3): $\delta = 0.90$ (br.), 1.15–1.48 (m, br.), 1.71 (m, br.), 2.80 (br.), 3.35 (br.), 3.64 (br.), 6.95 (br.) ppm. $^{13}\text{C}\{^1\text{H}\}$ NMR (CDCl_3): 14.2, 22.8, 29.4, 29.6, 30.6, 31.8, 66.5, 128.7, 130.6, 133.8, 134.2, 140.0 ppm. UV/Vis (CHCl_3): $\lambda_{\text{max}} = 452$ nm; anal. calcd: N/S 0.43, found 0.40.

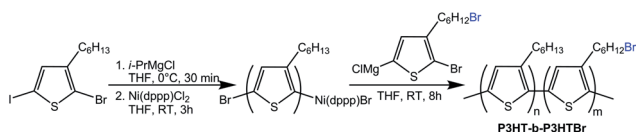
P3HT-*b*-P3HTPMe₃. Yield: 80%, ^1H NMR (CDCl_3): $\delta = 0.90$ (br.), 1.24–1.48 (br.), 1.70 (br.), 1.91 (br.), 2.12 (br.), 2.56 (br.), 2.80 (br.), 6.97 (br.) ppm. $^{13}\text{C}\{^1\text{H}\}$ NMR (CDCl_3): $\delta = 10.0, 10.3, 15.2, 22.8, 23.6, 23.8, 30.4, 30.2, 30.7, 31.4, 31.7, 32.7, 32.9, 129.7, 131.7, 134.8, 141.0$ ppm. $^{31}\text{P}\{^1\text{H}\}$ NMR (CDCl_3): $\delta = 27.0$ (s, 1P) ppm. UV/Vis (CHCl_3): $\lambda_{\text{max}} = 455$ nm.

Results and discussion

Polymer synthesis

The cationic diblock copolythiophenes were synthesised by a two-step procedure, similar to the analogous random copolymers and homopolymers.^{8,14} In the first step, the preparation of the regioregular head-to-tail bromide-bearing copolythiophene (P3HT-*b*-P3HTBr) in a 50/50 block ratio is achieved by using KCTP polymerisation (Scheme 1).^{24,34}

The P3HT block was first synthesised by polymerisation of 2-bromo-3-hexyl-5-iodothiophene with the Ni catalyst to obtain the end-living P3HT polymer. Subsequently, a new portion of activated 2,5-dibromo-3-bromohexylthiophene monomer was added to the reacting solution to obtain the final diblock copolymer P3HT-*b*-P3HTBr. After the polymerisation, the reaction mixture was quenched with 5 M HCl, following the procedure described by Yokozawa *et al.*³⁵ This quenching procedure



Scheme 1 Synthetic route applied toward the P3HT-*b*-P3HTBr precursor block copolymer.

prevents the polymer chains from undergoing dimerisation, in order to maintain the narrow polydispersity while efficiently removing inorganic impurities from the product.

Fig. 1 shows the SEC profiles of the P3HT block synthesised in the first step and the final diblock copolymer P3HT-*b*-P3HTBr after the second-stage polymerisation. Compared to the elution profile of the P3HT block obtained after the first step, the peak of the final diblock copolythiophene shifts to shorter elution volume (corresponding to a higher molecular weight), whilst maintaining a single peak, indicating the 'living' character and the formation of the diblock copolymer. A number-averaged molecular weight (M_n) of 11 000 g mol^{-1} and a polydispersity index (M_w/M_n) of <1.3 were obtained from the monomodal trace of the P3HT-*b*-P3HTBr copolymer in the SEC analysis.

MALDI-ToF analysis of P3HT-*b*-P3HTBr confirmed the covalent association of 3-bromohexylthiophene and 3-hexylthiophene. Indeed, the presence of m/z 166 and m/z 244 mass differences confirmed the presence of both monomer units inside the polymer chains (see Fig. S1 in the ESI†). However, the exact nature of the end-groups cannot be determined since, for instance, $\text{H}(3\text{HT})_x-(3\text{HTBr})_y-\text{Br}$ is an isomer of $\text{H}(3\text{HT})_{x-1}-(3\text{HTBr})_{y+1}-\text{H}$ and $\text{Br}(3\text{HT})_{x+1}-(3\text{HTBr})_{y-1}-\text{Br}$. An absolute averaged molecular weight of 7980 g mol^{-1} was determined by MALDI. Such a difference between the molecular weights obtained by SEC and MALDI is not unusual since GPC usually overestimates the molecular weight of rigid-rod poly(3-alkylthiophenes) by a factor of 1.2–2.3.^{20,36} The composition of the diblock copolythiophene was determined from the ^1H NMR spectra (Fig. S2†). The peaks observed at δ 0.90 and 3.42 ppm have been assigned to the resonance of the terminal methyl groups in the P3HT block and the methylene groups adjacent to the bromine atoms in the P3HTBr block, respectively. From the integration of these two peaks, the molar ratio of the P3HT and P3HTBr segments was 58 : 42, which is very close to the feed molar ratio of 55 : 45. The final step towards the diblock copolyelectrolytes P3HT-*b*-CPE involved the quaternization of the P3HT-*b*-P3HTBr precursor with 1-methyl-imidazole, pyridine, trimethylamine or trimethylphosphine (Scheme 2).

The efficiency of the conversion was monitored by ^1H NMR spectroscopy by following the shift of the terminal methylene group α of bromine at ~ 3.4 ppm (in CDCl_3) for the precursor

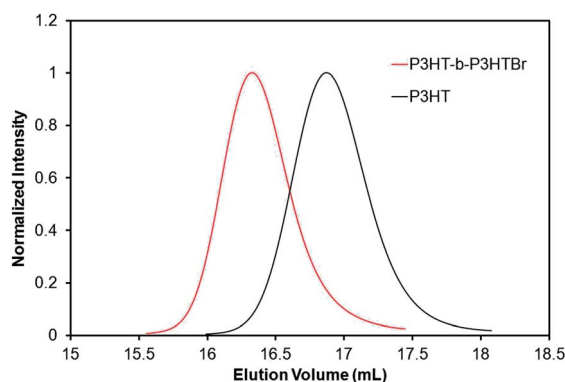
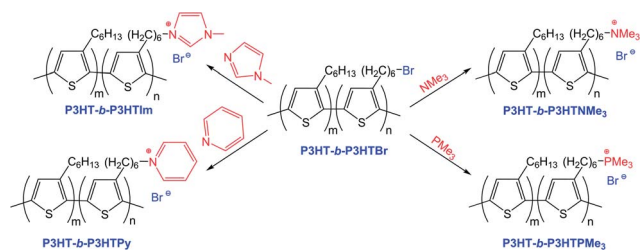


Fig. 1 SEC profiles obtained during the synthesis of the P3HT-*b*-P3HTBr block copolymer.



Scheme 2 Synthesis of the polyelectrolyte diblock copolymers **P3HT-*b*-CPE** (CPE = **P3HTIm**, **P3HTPy**, **P3HTNMe₃**, and **P3HTPMe₃**).

copolymer. Based on ¹H NMR spectroscopy, the quaternisation appears to be quantitative. It was also confirmed by the *N/S* ratio values obtained from elemental analysis for the ionic diblock copolymers containing cationic nitrogen side groups which are very close to the expected values calculated on the basis of the composition of the precursor diblock copolymer.

Thermal properties

In Rapid Heat–Cool (RHC) calorimetry measurements, an important endothermal effect can be observed during the first heating of all four materials, indicating the presence of a significant amount of water or solvent that evaporates upon heating. Such an effect is no longer present during the second heating, where a glass transition temperature (*T_g*) significantly above room temperature is observed for the four materials. The endothermal effect appears again when the copolymers are stored in the non-hermetic RHC crucibles under ambient conditions, proving water vapour absorption and indicating the materials' hydrophilicity.

Fig. 2 shows this behaviour for **P3HT-*b*-P3HTPMe₃**. As this effect is also present in the pure **P3HTPMe₃** polymer, it can be concluded that it is caused by the CPE block and can be linked to the bromide counterion.¹⁴ This is an important finding for

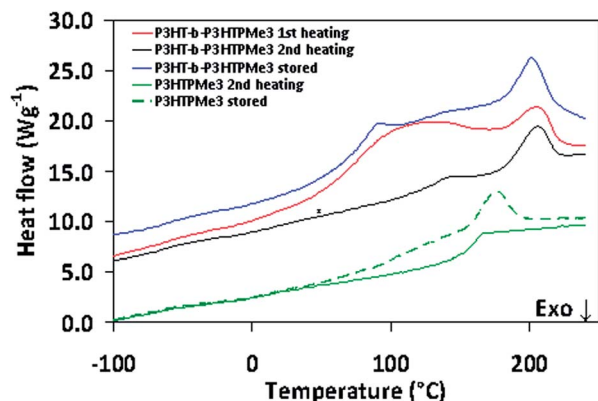


Fig. 2 RHC thermogram of **P3HT-*b*-P3HTPMe₃** showing the first heating (red) and the second heating (black). After storage under ambient conditions, a curve similar to that of the first heating is found (blue). Thermograms of the second heating and after storage under ambient conditions are also included for pure **P3HTPMe₃** for comparison (dashed and solid green). The curves are shifted vertically for clarity.

potential applications, as water vapour absorption will drastically lower the *T_g* of this block if the material is not used under dry conditions.³⁷ When comparing the second heating runs of the different **P3HT-*b*-CPE** polymers, a melting peak is observed at a similar temperature (around 205 °C) for all materials except **P3HT-*b*-P3HTNMe₃**. These melting transitions can be attributed to the **P3HT** block, which is known to be a fast-crystallising conjugated polymer. A clear *T_g* is also always present, caused by the CPE block, as can be seen by comparing with the pure CPE materials. The CPE block *T_g* and the melting point (*T_m*) and enthalpy (ΔH_m) of the **P3HT** block are summarised for the four copolymers in Table 1.

The thermal transitions observed by RHC during the second heating run are confirmation of the diblock copolymer architecture of the synthesised materials. The nature of the CPE block can modify its *T_g* by approximately 100 °C, ranging from 57 °C up to 159 °C. The thermogram of **P3HT-*b*-P3HTNMe₃** (Fig. 3) clearly shows that the **P3HT** melting transition differs for this material.

In this case, the *T_g* of the **P3HTNMe₃** block overlaps with the **P3HT** melting peak, and this high *T_g* value around 159 °C is expected to strongly inhibit the crystallisation process of the **P3HT** block. Indeed, in the temperature region of **P3HT** crystallisation during cooling, the **P3HTNMe₃** block can impose severe mobility restrictions by concurrent vitrification. This results in a lower melting temperature and enthalpy of the **P3HT** block. In contrast, the other **P3HT-*b*-CPE** copolymers do not show this behaviour, such as *e.g.* **P3HT-*b*-P3HTIm** (see Fig. 3). Interestingly, the pure **P3HTIm** polymer seems to be somewhat crystalline, showing a small melting peak at about 196 °C (in close vicinity to the **P3HT** melting). This explains the slightly higher melting enthalpy found for the **P3HT-*b*-P3HTIm** copolymer, when compared to the other materials. It should be noted that the thermograms of Fig. 3 and the values of Table 1 are indicative and demonstrate the trends of the different **P3HT-*b*-CPE** polymers during the second heating for the applied RHC conditions. The position of *T_g* and *T_m* and the melting enthalpy ΔH_m strongly depend on all experimental conditions, *i.e.* the synthesis procedure (sequence of block synthesis, precise block length control and resulting PDI of blocks, regioregularity of **P3HT**, nature of end-groups), the purification and the eventual drying (vacuum at 40 °C) and storage. Moreover, the solvent dependent assembly of the block

Table 1 Glass transition (*T_g*) of the CPE block and melting temperature (*T_m*) and enthalpy (ΔH_m) of the **P3HT** block for all **P3HT-*b*-CPE** materials measured by RHC during the second heating run

Polymer	<i>T_g</i> (°C)	<i>T_m</i> (°C)/ ΔH_m (J g ⁻¹)
P3HT-<i>b</i>-P3HTIm	57	206/13.1
P3HT-<i>b</i>-P3HTPy	75	204/10.2
P3HT-<i>b</i>-P3HTNMe₃	159 ^a	177/7.3
P3HT-<i>b</i>-P3HTPMe₃	136	205/9.2

^a Due to the overlap with the melting peak of the **P3HT** block, the *T_g* of the **P3HTNMe₃** block could not be determined in the block copolymer; instead, the value of the pure **P3HTNMe₃** polymer is given.

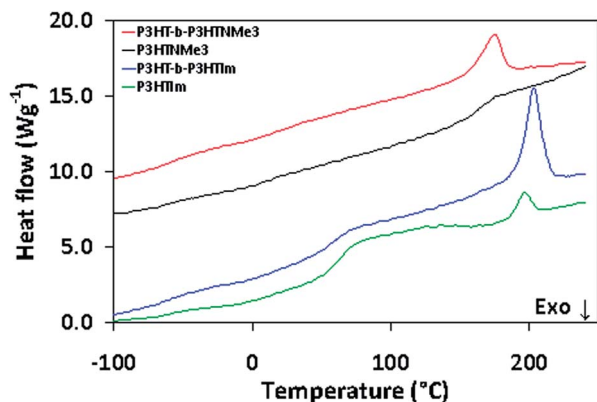


Fig. 3 RHC thermogram of P3HT-*b*-P3HTNMe₃ (red) and P3HT-*b*-P3HTIm (blue), showing the second heating. For comparison, the second heating of the P3HTNMe₃ (black) and P3HTIm (green) pure polymers is shown. The curves were shifted vertically for clarity.

copolyelectrolytes and the persistence of the solvent-induced nanomorphology after removal of the solvent are probably important for the thermal properties and their stability as well (see further in 'Aggregation behaviour' as studied by DLS, SANS, and AFM). As an example, the thermal properties of P3HT-*b*-P3HTIm are still evolving in subsequent cool-heat cycles after the second heating; T_g is raised from 57 °C to above 70 °C after 10 cycles, while T_m decreases from 206 °C towards 180 °C in combination with a lowered ΔH_m from 13.1 J g⁻¹ to 8.5 J g⁻¹. These findings suggest further changes in the nanomorphology as a result of thermal cycling, leading to a loss of perfection of the P3HT crystals, possibly with a concomitant loss of a minor amount of residual solvent from the ionic block. Similar effects are noticed for the other P3HT-*b*-CPE polymers.

Solution behaviour

The optical properties of the cationic P3HT-*b*-CPE copolymers in solution have been studied by UV/Vis absorption and photoluminescence (PL) spectroscopy. The neutral diblock copolymer P3HT-*b*-P3HTBr exhibits a broad absorption band with a maximum (λ_{max}) centred at 450 nm in chloroform (CHCl₃), which, as expected, is similar to the parent P3HT. After functionalisation with the imidazolium, pyridinium, trimethylammonium or trimethylphosphonium moieties, the P3HT-*b*-CPE polymers also become soluble in more polar solvents such as water and MeOH due to the presence of the hydrophilic pendant ionic side groups which overcome the hydrophobic π - π stacking interactions between the polythiophene backbones. We note that P3HT-*b*-P3HTPy is somewhat less soluble in these solvents than its P3HT-*b*-CPE counterparts, indicating the somewhat reduced hydrophilic (or increased hydrophobic) character of the P3HTPy block, as previously reported by Scherf *et al.* for the polyfluorene (PF2/6)-polythiophene diblock copolyelectrolyte analogue PF2/6-P3HTPy.^{12a} P3HT-*b*-CPE copolymers exhibit solvatochromatic behaviour, appearing dark red/brown in CHCl₃ and dark violet in methanolic and aqueous solution (Fig. 4a and S13-S15†). This solvatochromatism is reflected in the corresponding UV/Vis absorption spectra, as

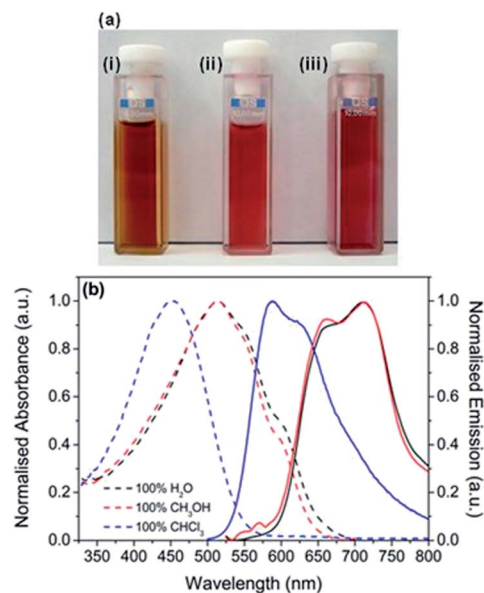


Fig. 4 (a) P3HT-*b*-P3HTPMe₃ in (i) CHCl₃, (ii) MeOH and (iii) H₂O. (b) Corresponding normalised UV/Vis absorption and emission spectra of P3HT-*b*-P3HTPMe₃ in 100% CHCl₃ (blue), 100% H₂O (black) and 100% MeOH (red).

shown in Fig. 4b for P3HT-*b*-P3HTPMe₃ where λ_{max} red-shifts from ~450 nm in CHCl₃ to ~520 nm in H₂O and MeOH, with the additional emergence of a vibronic structure in the latter solvents.

P3HT has previously been reported to self-assemble into a lamellar-like structure built from interchain π - π stacking interactions between the planarised aromatic backbones of the polymer chains.³⁸ This supramolecular organisation is accompanied by a bathochromic shift in the absorption spectrum and the vibronic structure at longer wavelengths, very similar to the behaviour observed here for P3HT-*b*-CPEs in MeOH and water. Water is expected to be a non-solvent for the hydrophobic, neutral P3HT block, with only low to moderate solubility anticipated in MeOH. We propose that the significant bathochromic shift is indicative of increased aggregation of the hydrophobic P3HT block in these poor solvents. The concomitant appearance of the vibronic structure further suggests increased confinement and/or planarisation of one or both of the blocks, thereby hindering free rotation of thiophene units along the polymer backbone. The P3HT-*b*-CPE copolymers are weakly fluorescent in solution and the emission spectra exhibit similar solvatochromatic trends (Fig. 4b). A significant red-shift in the emission maximum (λ_{em}) from 588 nm to 711 nm is observed for P3HT-*b*-P3HTPMe₃ upon changing the solvent from CHCl₃ to MeOH or H₂O, which is again accompanied by the increased vibronic structure assigned to the vibronic progression of the C=C stretching mode ($\Delta E \approx 0.15$ eV).³⁹ The optical properties are similar for all copolymers in the P3HT-*b*-CPE series and absorption and photoluminescence maxima in each solvent are collected in Table 2. The use of solvent mixtures has been shown to be very effective for both breaking up the aggregates formed by homopolymer CPEs in aqueous

Table 2 Absorption and photoluminescence maxima (λ_{max}) of the P3HT-*b*-CPE diblock copolymers in various solvents (PL excitation wavelength: 523 nm)

Polymer	Absorption (λ_{max} /nm)			Emission (λ_{max} /nm)		
	CHCl ₃	MeOH	H ₂ O	CHCl ₃	MeOH	H ₂ O
P3HT- <i>b</i> -P3HTIm	452	519	522	586	729	729
		556	625			
P3HT- <i>b</i> -P3HTPy	455	517	520	580	721	723
		556	619			
		607				
P3HT- <i>b</i> -P3HTNMe ₃	452	518	518	592	721	722
		556	631			
		607				
P3HT- <i>b</i> -P3HTPMe ₃	455	516	516	588	707	710
		556	627			
		607				

solution⁴⁰ and controlling segregation and self-organisation of diblock copolymers.^{12,13}

The UV/Vis absorption and PL properties of P3HT-*b*-CPE copolymers were thus further examined in MeOH-H₂O solvent mixtures from 0–100% (v/v), as illustrated in Fig. 5 for P3HT-*b*-P3HTPy and in Fig. S16–S18† for other P3HT-*b*-CPEs. The gradual increase in the volume of MeOH added to an aqueous solution of P3HT-*b*-P3HTPy is accompanied by a concomitant increase in the absorbance, which reaches its maximum value at 50% (v/v) MeOH-H₂O; above this, the absorbance drops off once again (Fig. 5a, inset). A similar trend is observed in the corresponding PL spectrum, with the emission intensity again reaching its upper limit at 50% (v/v) MeOH-H₂O (Fig. 5b). Notably, no shift in the absorption or emission maximum wavelength was observed for any of the solvent mixtures studied.

Fluorescence quantum yields (Φ_{F}) were determined to quantify the extent of the fluorescence enhancement in each solvent mixture (Fig. 6a). For P3HT-*b*-P3HTPy, P3HT-*b*-P3HTNMe₃ and P3HT-*b*-P3HTPMe₃, $\Phi_{\text{F}} \sim 0.5\%$ in 100% MeOH and $\Phi_{\text{F}} \sim 1.0\text{--}1.5\%$ in 100% H₂O were obtained. As the ratio of

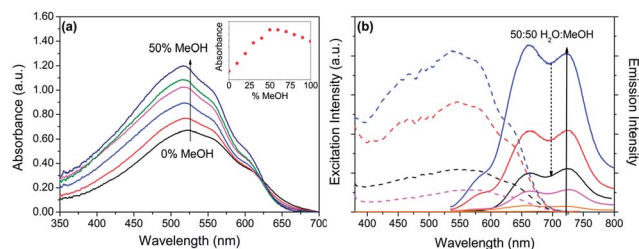


Fig. 5 (a) UV/Vis absorption spectra of P3HT-*b*-P3HTPy in H₂O–MeOH solvent mixtures. Inset: absorbance at 522 nm (λ_{max}) as a function of vol% MeOH in H₂O–MeOH mixtures. (b) Selected excitation ($\lambda_{\text{em}} = 730$ nm) and PL ($\lambda_{\text{ex}} = 515$ nm) spectra of P3HT-*b*-P3HTPy in 100% MeOH (orange line), 70% MeOH (violet line), 50% MeOH (blue line), 30% MeOH (red line) and 0% MeOH (black line).

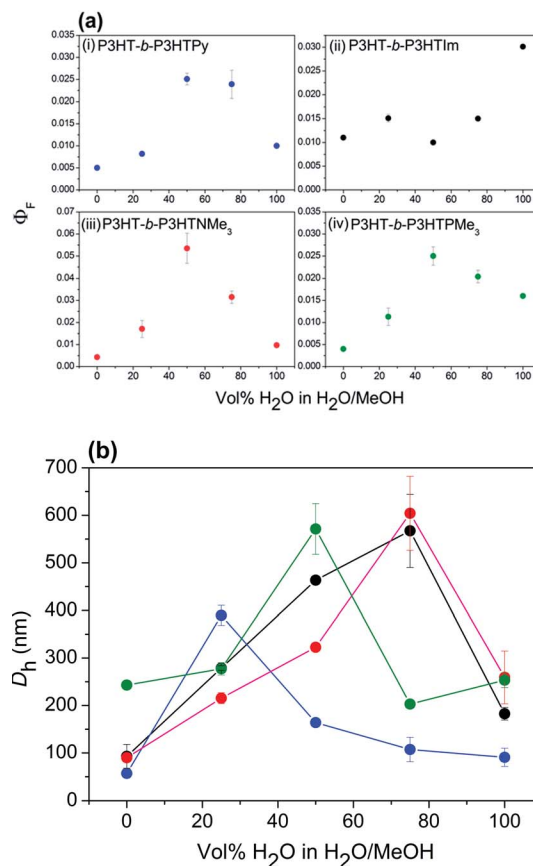


Fig. 6 (a) Fluorescence quantum yields (Φ_{F}) and (b) hydrodynamic diameter (D_{h} , Z-average) of P3HT-*b*-CPEs in H₂O–MeOH solvent mixtures (0.35 $\mu\text{g mL}^{-1}$). Legend: P3HT-*b*-P3HTPy (blue circles), P3HT-*b*-P3HTIm (black circles), P3HT-*b*-P3HTNMe₃ (red circles) and P3HT-*b*-P3HTPMe₃ (green circles). The solid lines serve only to guide the eye.

solvents in the mixture is varied, Φ_{F} gradually increases, reaching a maximum of $\Phi_{\text{F}} \sim 5.5\%$ in 50% (v/v) MeOH-H₂O. P3HT-*b*-P3HTIm exhibits a slightly different trend; Φ_{F} remains constant at $\sim 1.0\text{--}1.5\%$ across the range 100% MeOH to 20 : 80% (v/v) MeOH-H₂O, before doubling to $\Phi_{\text{F}} \sim 3\%$ in 100% H₂O. The increase in the fluorescence quantum yield in the mixed solvent system suggests improved solubilisation and at least, partial isolation of polymer chains in one or both the blocks.

Aggregation behaviour

The aggregation behaviour of P3HT-*b*-CPEs in solution and thin films was further investigated by dynamic light scattering (DLS), small-angle neutron scattering (SANS) and atomic force microscopy (AFM). DLS analysis was initially performed to determine the average hydrodynamic diameter (D_{h}) of P3HT-*b*-CPE aggregates in MeOH-H₂O mixtures (Fig. 6b). Samples typically exhibited a monomodal distribution of low polydispersity in all solvent mixtures investigated. The smallest aggregates were obtained in 100% MeOH (~ 100 nm for P3HT-*b*-P3HTNMe₃, P3HT-*b*-P3HTIm, and P3HT-*b*-P3HTPy and

~ 250 nm for **P3HT-*b*-P3HTPMe₃**), with slightly larger aggregates found in 100% H₂O (~ 100 nm for **P3HT-*b*-P3HTPy**, ~ 200 – 260 nm for **P3HT-*b*-P3HTIm** and **P3HT-*b*-P3HTPMe₃**, and ~ 300 nm for **P3HT-*b*-P3HTNMe₃**). The largest D_h values (~ 400 – 600 nm) were consistently obtained in ~ 40 – 60% (v/v) MeOH–H₂O, which is consistent with increased solubility of both the neutral **P3HT** block and the charged CPE block in the mixed solvent systems, resulting in swelling of the aggregate structure due to associated solvent molecules.

To obtain deeper insight into the particle shape and nano-scale organisation in solution, small-angle neutron scattering (SANS) studies were performed on **P3HT-*b*-P3HTIm** and **P3HT-*b*-P3HTPy** in deuterated solution. Fig. 7 plots the SANS data for **P3HT-*b*-P3HTPy** in D₂O, *d*₄-MeOD and their 50 : 50 (v/v) mixture (corresponding plots for **P3HT-*b*-P3HTIm** are shown in Fig. S22 in the ESI†). All three solvents yield similar scattering profiles with a shoulder at $q = 0.02 \text{ \AA}^{-1}$ and an upturn at $q = 0.008 \text{ \AA}^{-1}$; however they do differ in the gradient of their slopes. At high q ($q > 0.07 \text{ \AA}^{-1}$), the SANS response stems from the internal structure of the aggregate. The excess scatter for some samples at $q \sim 0.1$ – 0.2 \AA^{-1} is likely due to the internal structure within the aggregates, perhaps due to repulsive interactions between similarly charged polymer chains.^{5a-c} The upturn in $I(q)$ at $q < 0.008 \text{ \AA}^{-1}$ is indicative of particle aggregation. The power law scaling for the intermediate q region ($0.02 < q < 0.07$) varies from $q^{-4.2}$ in *d*₄-MeOD to $q^{-5.21}$ in D₂O. The low q region ($q < 0.02$) decays as $\sim q^{-5/3}$, which is typical of scattering from either cylindrical aggregates or from individual chains.⁴¹ The observation window of these SANS experiments ranged from 2–160 nm, which is well beyond the isolated chain length (22.7–25.4 nm). Unique fits to the SANS data were not possible; however all those chosen (Table S1 in the ESI†) have absolute SANS intensities consistent with the known sample concentrations (~ 1 vol% dry material). All the fits show that the

aggregates must contain upwards of 30% solvent, without any significant “dry core”. Better fits were obtained with a core plus shell model with a diffuse outer shell containing 85–95% solvent. The exception to the latter were the samples in pure MeOD, where a thin shell (of ~ 2 nm) seems to have slightly less solvent (~ 65 vol%) than the core of the aggregate (~ 80 vol% solvent). The SANS data from the aggregates in MeOD are also more consistent with an elongated, rod-like structure, whilst the others are better fit as discs. The disc cases would also be equally well fitted as core-shell ellipsoids or as rather poly-disperse core-shell spheres. There is no clear evidence in the SANS patterns of a sharp core-shell boundary, so a continuous radial variation in the solvent composition seems likely, though this would be more difficult to model. Aggregation numbers are likely in the range ~ 100 to ~ 300 copolymer chains.

The SANS data ($0.0046 < q < 0.6$) in each solvent were fitted to a Core-Shell-Cylinder model using a non-linear least-squares method, including polydispersity and q -resolution smearing (fits shown as solid lines in Fig. 7).³³ For **P3HT-*b*-P3HTPy** in *d*₄-MeOD, depending on the starting imputed values of length and radius, the fits were found to converge to two slightly differing shapes: (1) a rod with a core length, L_{core} , of ~ 80 nm, a core radius, r_{core} , of ~ 6 nm and a shell thickness, T_{shell} , of ~ 2 nm; (2) a disc with $L_{\text{core}} \sim 75$ nm, $r_{\text{core}} \sim 30$ nm and $T_{\text{shell}} \sim 1$ nm. The rod-like core-shell aggregate (1) resulted in an improved fit at low q (Fig. 7, inset). The SANS data for **P3HT-*b*-P3HTPy** in 50 : 50 (v/v) *d*₄-MeOD–D₂O were also best modelled by a disc-like core-shell aggregate, revealing a wet core with $L_{\text{core}} \sim 11$ nm and $r_{\text{core}} \sim 7.5$ nm, and a thick solvated shell ($T_{\text{shell}} \sim 9.5$ nm). Fitting the SANS data of **P3HT-*b*-P3HTPy** in D₂O similarly yielded a disc with a solvated core ($L_{\text{core}} \sim 9$ nm and $r_{\text{core}} \sim 6$ nm) and a very wet shell of $T_{\text{shell}} \sim 8$ nm. The shell thickness corresponds to the fully extended length of the charged **P3HTPy** block. Therefore it is likely that the drier core corresponds to the aggregated neutral **P3HT** blocks. We note that reasonable fits to the SANS data in D₂O and 50 : 50 (v/v) *d*₄-MeOD–D₂O could also be obtained with a Core-Shell Sphere model, which yielded aggregates of similar dimensions to those described above (Table S2 in the ESI†). Similar fits were obtained for **P3HT-*b*-P3HTIm** and can be found with the tabulated summaries of the fitting data for both CPEs in the ESI.†

The scattering length densities (SLDs) of the neutral and charged CPE blocks are both $\sim 1.1 \times 10^{-6} \text{ \AA}^{-2}$. Therefore, they can only be distinguished by neutron scattering when one block is substantially more solvated than the other. The SANS data fits for **P3HT-*b*-P3HTPy** in D₂O suggest the presence of aggregates with a highly swollen shell. Since D₂O is expected to be a selective solvent for the charged CPE block, we propose that the aggregate core consists predominantly of the neutral **P3HT** blocks, surrounded by a highly solvated CPE shell. Since D₂O is a non-solvent for **P3HT**, the hydrophobic effect results in tight packing of the **P3HT** chains within the aggregate core to minimise the interaction with the solvent. In 50 : 50 (v/v) *d*₄-MeOD–D₂O, the core-shell aggregate structure is retained, but the solvent mixture results in improved solvation of both blocks, leading to an increase in both the core radius and shell thickness. In MeOD, **P3HT-*b*-P3HTPy** forms elongated core-shell

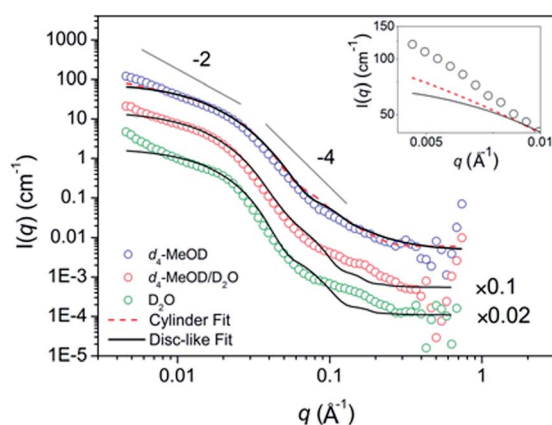


Fig. 7 SANS data for **P3HT-*b*-P3HTPy** in *d*₄-MeOD, 50 : 50 (v/v) *d*₄-MeOD–D₂O and D₂O (10 mg mL⁻¹). For clarity, the *d*₄-MeOD–D₂O and D₂O data have been offset by 0.1 and 0.02, respectively. Straight lines show -2 and -4 decays for comparison. The solid black lines show the disc-like fits obtained using the Core-Shell-Cylinder model for each solvent mixture. Only **P3HT-*b*-P3HTPy** in *d*₄-MeOD was found to be better fit by rods at low q , as shown by the red dashed line in the inset.

cylindrical structures, with a solvated core and a drier shell. On the basis of the Hildebrand solubility parameters, MeOH is a relatively poor solvent for **P3HT** ($\delta \sim 19.1 \text{ MPa}^{1/2}$ for **P3HT** and $\delta \sim 29.7 \text{ MPa}^{1/2}$ for MeOH, respectively⁴²) and should be a better solvent for the charged CPE block. We propose that in MeOH, **P3HT-*b*-P3HTPy** forms core-shell aggregates in which the **P3HT** blocks predominantly occupy the core, but cannot exclude partial mixing of the two blocks across both domains. In the future we would like to deuterate the side chains of the **P3HT** blocks in order to obtain unequivocal evidence for the location of the blocks from SANS.

Atomic force microscopy was used to determine whether the structured aggregates formed in solution could be transferred as thin films with the retention of their nanoscale organisation, which is a key requirement for potential device applications. Solutions of **P3HT-*b*-P3HTIm** at low concentrations ($3.5\text{--}7.0 \mu\text{g mL}^{-1}$) drop cast onto mica substrates reveal the occurrence of spheroids whose surface morphology and size critically depend on the deposition solvent. In MeOH, a honeycomb-like texture is observed on the aggregate surface (Fig. 8a), with an average diameter of $128 \pm 28 \text{ nm}$. The surface texture may be indicative of the fusion of several smaller structures into larger aggregates. In water, slightly larger, isolated aggregates are observed (average diameter $\sim 147 \pm 28 \text{ nm}$), whose surface morphology is much smoother (Fig. 8b). In 50% (v/v) MeOH-H₂O, amorphous films formed from extended networks of much smaller, disc-like clusters, 50–80 nm in diameter, are observed (Fig. 8c). Similar trends are observed for all **P3HT-*b*-CPEs** (Fig. S20 and S21 in the ESI†). It should be noted that the SANS data indicate that the core-shell aggregates formed in solution are highly solvated; in contrast the corresponding thin film samples were dried prior to AFM imaging. It is conceivable that removal of the solvent during drying may lead to partial collapse or

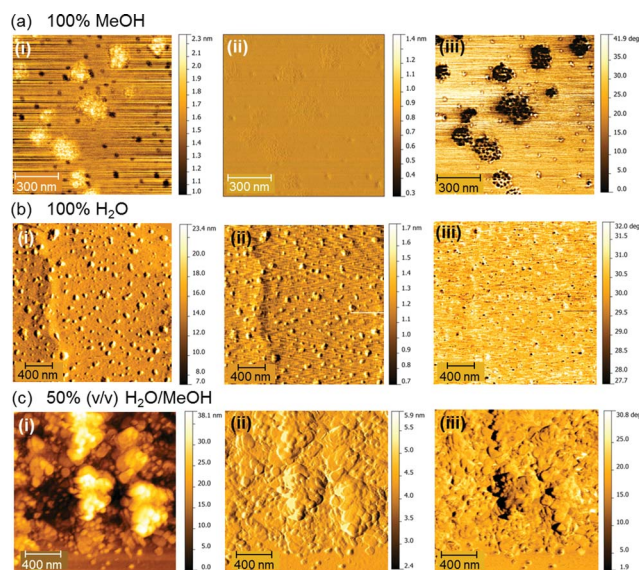


Fig. 8 AFM tapping mode images of **P3HT-*b*-P3HTIm** films drop-cast from (a) 100% MeOH ($7 \mu\text{g mL}^{-1}$), (b) 100% H₂O ($3.5 \mu\text{g mL}^{-1}$) and (c) 50% (v/v) H₂O–MeOH ($3.5 \mu\text{g mL}^{-1}$) onto freshly cleaved mica: (i) height, (ii) amplitude and (iii) phase images, respectively.

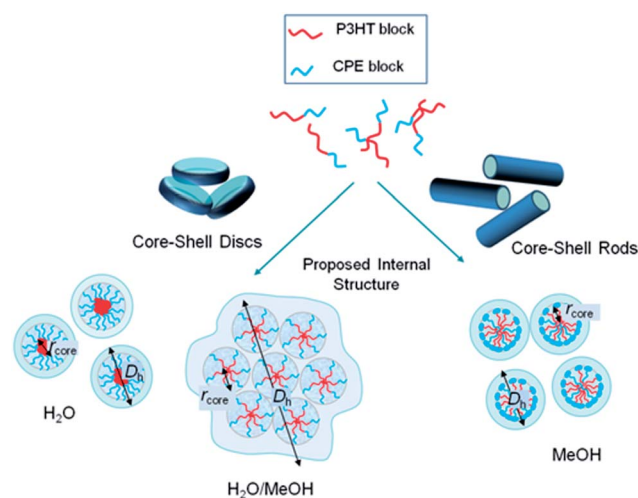


Fig. 9 Schematic representation of the proposed internal aggregate structures of **P3HT-*b*-CPE** in H₂O, MeOH and H₂O–MeOH mixtures. L_{core} , r_{core} and T_{shell} are the core length, core radius and shell thickness obtained from SANS data fitting, respectively. D_{h} is the hydrodynamic diameter measured by DLS. We note that the precise arrangement of the **P3HT** and CPE block domains in the aggregates formed in MeOH is still undetermined.

reorganisation of the aggregate structure due to fluctuations in the solvent gradient.

Fig. 9 shows a schematic representation of the proposed aggregate structures adopted by **P3HT-*b*-CPEs** in H₂O, MeOH and H₂O–MeOH mixtures. The smallest aggregates are formed in pure MeOH (DLS, SANS, and AFM) and exhibit a core-shell cylindrical structure comprised of a long, “wet” core, protected by a “dry” thin shell. MeOH is a poor solvent for **P3HT**, which is anticipated to predominantly occupy the aggregate core; however we cannot exclude some mixing of the **P3HT** and CPE blocks across both the core and shell domains. The small aggregate size results in increased chain proximity and inter-chain exciton migration, resulting in the lowest Φ_{F} values being obtained in this solvent. Slightly larger aggregates are obtained in pure H₂O (DLS, AFM, and SANS) and consist of a drier core of aggregated, neutral **P3HT** blocks and a wet shell of well-dissolved CPE chains. The largest aggregates are formed in MeOH–H₂O mixtures (DLS and SANS), in which the core and shell are both well-solvated. This is in excellent agreement with the corresponding increase in the Φ_{F} values observed in MeOH–H₂O mixtures. Moreover, due to the higher solubility of the entire CPE chain, we expect lower aggregation numbers for each structure, thereby reducing electrostatic repulsion between the highly solvated, individual chains from which each aggregate is comprised. Reduced electrostatic repulsion may result in long-range assembly of multiple aggregates, which may explain the large D_{h} obtained by DLS and the textured extended sheets (rather than individual clusters) observed by AFM.

Conclusions

Amphiphilic rod-rod diblock copolymers containing a hydrophobic **P3HT** block and a hydrophilic cationic **P3HT** block

bearing different side groups were synthesised in an efficient way by using Kumada catalyst-transfer polycondensation. In contrast to the neutral parent polymer **P3HT-*b*-P3HTBr**, the incorporation of cationic terminal groups renders **P3HT-*b*-CPES** soluble in highly polar solvents. The thermal properties of these copolymers indicate a clear signature of the diblock architecture by the presence of a T_g caused by the CPE block and a T_m corresponding to the **P3HT** block. The nature of the CPE block drastically affects the T_g , and to a lesser extent the melting transition of the **P3HT** block, except in the case of **P3HT-*b*-P3HTNMe₃**. The UV/Vis absorption and photoluminescence properties are solvent-dependent, resulting in a significant bathochromic shift in λ_{max} , increased vibronic structure and a decrease in the fluorescence quantum yield in pure MeOH and H₂O, which is attributed to aggregate formation. Fluorescence quantum yields are enhanced in H₂O–MeOH mixtures, which are accompanied by an analogous trend in the Z-average particle diameter determined by DLS. Small-angle neutron scattering data are consistent with the fact that **P3HT-*b*-CPES** form core–shell discs or cylinders in solution, with the relative thickness and “wetness” of the core and the shell determined by the solvent system. In H₂O–MeOH mixtures, we propose that enhanced solvation of both the core and shell results in aggregate swelling, which promotes disaggregation of localised polymer chains, thereby increasing Φ_F . AFM studies reveal that the aggregates formed in solution can be transferred as thin films.

Acknowledgements

The authors thank the CNRS and the Université Montpellier II for financial support. This research has been supported by the European Commission under the 7th Framework Programme through the ‘Research Infrastructures’ action of the ‘Capacities’ programme. Contract no.: CP-CSA_INFRA-2008-1.1.1 number 226507-NM13. We thank ISIS and STFC for the allocation of SANS Xpress beamtime. Research in Mons is supported by the Science Policy Office of the Belgian Federal Government (BEL-SPO; PAI 7/05), FNRS-FRFC and Région Wallonne (OPTI2MAT excellence programme). The authors are also grateful to National Fund for Scientific Research (F.R.S.-FNRS) in the frame of the FRFC research program (convention no. 2.4508.12). The MS laboratory acknowledges the “Fonds de la Recherche Scientifique (FRS-FNRS)” for its contribution to the acquisition of the Waters QToF Premier Mass Spectrometer. J.D.W. thanks FRS-FNRS (convention no. 2.4508.12) for financial support.

Notes and references

- 1 *Conjugated polyelectrolytes. Fundamentals and Applications*, ed. B. Liu and G. C. Bazan, Wiley-VCH, Weinheim, 2013.
- 2 (a) W. Lee, J. H. Seo and H. Y. Woo, *Polymer*, 2013, **54**, 5104; (b) A. Duarte, K.-Y. Pu, B. Liu and G. C. Bazan, *Chem. Mater.*, 2011, **23**, 501; (c) H. Jiang, P. Taranekekar, J. R. Reynolds and K. S. Schanze, *Angew. Chem., Int. Ed. Engl.*, 2009, **48**, 4300; (d) C. Zhu, L. Liu, Q. Yang, F. Lv and S. Wang, *Chem. Rev.*, 2012, **112**, 4687; (e) G. Feng, J. Liang and B. Liu, *Macromol. Rapid Commun.*, 2013, **34**, 705; (f) G. Feng, D. Ding and B. Liu, *Nanoscale*, 2012, **4**, 6150.
- 3 (a) T.-Q. Nguyen, R. C. Kwong, M. E. Thompson and B. J. Schwartz, *Appl. Phys. Lett.*, 2000, **76**, 2454; (b) C. L. Chochos and S. A. Choulis, *Prog. Polym. Sci.*, 2011, **36**, 1326; (c) K. Vandewal, S. Himmelberger and A. Salleo, *Macromolecules*, 2013, **46**, 6379.
- 4 R. C. Evans, *J. Mater. Chem. C*, 2013, **1**, 4190 and references therein.
- 5 (a) M. Knaapila, R. C. Evans, V. M. Garamus, L. Almásy, N. K. Székely, A. Gutacker, U. Scherf and H. D. Burrows, *Langmuir*, 2010, **26**, 15634; (b) M. Knaapila, R. C. Evans, A. Gutacker, V. M. Garamus, N. K. Székely, U. Scherf and H. D. Burrows, *Soft Matter*, 2011, **7**, 6863; (c) R. C. Evans, M. Knaapila, N. Willis-Fox, M. Kraft, A. Terry, H. D. Burrows and U. Scherf, *Langmuir*, 2012, **28**, 12348; (d) Y.-M. Chang, R. Zhu, E. Richard, C.-C. Chen, G. Li and Y. Yang, *Adv. Funct. Mater.*, 2012, **22**, 3284; (e) M. E. H. Heeley, J. K. Gallaher, T. L. Nguyen, H. Y. Woo and J. M. Hodgkiss, *Chem. Commun.*, 2013, **49**, 4235.
- 6 H. Jiang, X. Zhao and K. S. Schanze, *Langmuir*, 2006, **22**, 5541.
- 7 (a) H. D. Burrows, S. M. Fonseca, F. B. Dias, J. Seila de Melo, A. P. Monkman, U. Scherf and S. Pradhan, *Adv. Mater.*, 2009, **21**, 1155; (b) J. E. Houston, A. R. Patterson, A. C. Jayasundera, W. Schmitt and R. C. Evans, *Chem. Commun.*, 2014, DOI: 10.1039/c3cc47552b.
- 8 J. Rubio-Magnieto, A. Thomas, S. Richeter, A. Mehdi, P. Dubois, R. Lazzaroni, S. Clément and M. Surin, *Chem. Commun.*, 2013, **49**, 5483.
- 9 (a) U. Scherf, A. Gutacker and N. Koenen, *Acc. Chem. Res.*, 2008, **41**, 1086; (b) P.-T. Wu, G. Ren, F. S. Kim, C. Li, R. Mezzenga and S. A. Jenekhe, *J. Polym. Sci., Part A: Polym. Chem.*, 2010, **48**, 614; (c) J. Kim, A. Siva, I. Y. Song and T. Park, *Polymer*, 2011, **52**, 3704; (d) Y. Lin, J. A. Lim, Q. Wei, S. C. B. Mannsfeld, A. L. Briseno and J. J. Watkins, *Chem. Mater.*, 2012, **24**, 622; (e) A. Yassar, L. Miozzo, R. Gironda and G. Horowitz, *Prog. Polym. Sci.*, 2013, **38**, 791; (f) M. J. Robb, S.-Y. Ku and C. J. Hawker, *Adv. Mater.*, 2013, **25**, 5686.
- 10 (a) Y. Zhang, K. Tajima, K. Hirota and K. Hashimoto, *J. Am. Chem. Soc.*, 2008, **130**, 7812; (b) Y. Zhang, K. Tajima and K. Hashimoto, *Macromolecules*, 2009, **42**, 7008.
- 11 (a) D. M. Vriezema, M. C. Aragonés, J. A. A. W. Elemans, J. J. L. M. Cornelissen, A. E. Rowan and R. J. M. Nolte, *Chem. Rev.*, 2005, **105**, 1445; (b) A. Kros, W. Jesse, G. A. Metselaar and J. J. L. M. Cornelissen, *Angew. Chem., Int. Ed.*, 2005, **44**, 4349; (c) R. Verduzco, I. Botiz, D. L. Pickel, S. M. Kilbey, K. Hong, E. Dimasi and S. B. Darling, *Macromolecules*, 2011, **44**, 530.
- 12 (a) G. Tu, H. Li, M. Forster, R. Heiderhoff, L. J. Balk, R. Sigel and U. Scherf, *Small*, 2007, **3**, 1001; (b) A. Gutacker, S. Adamczyk, A. Helfer, L. E. Garner, R. C. Evans, S. M. Fonseca, M. Knaapila, G. C. Bazan, H. D. Burrows and U. Scherf, *J. Mater. Chem.*, 2010, **20**, 1423; (c) A. Gutacker, N. Koenen, U. Scherf, S. Adamczyk, J. Pina, S. M. Fonseca, A. J. M. Valente, R. C. Evans, J. Seixas de Melo, H. D. Burrows and M. Knaapila, *Polymer*, 2010, **51**,

- 1898; (d) M. Knaapila, R. C. Evans, A. Gutacker, V. M. Garamus, M. Torkkeli, S. Adamczyk, M. Forster, U. Scherf and H. D. Burrows, *Langmuir*, 2010, **26**, 5056; (e) T. Ghooos, N. Van den Brande, M. Defour, J. Brassinne, C.-A. Fustin, J.-F. Gohy, S. Hoepfener, U. S. Schubert, W. Vanormelingen, L. Lutsen, D. J. Vanderzande, B. Van Mele and W. Maes, *Eur. Polym. J.*, 2014, **53**, 206.
- 13 (a) U. Scherf, R. C. Evans, A. Gutacker and G. C. Bazan, in *Conjugated polyelectrolytes. Fundamentals and Applications*, ed. B. Liu and G. C. Bazan, Wiley-VCH, Weinheim, 2013, pp. 65–90; (b) A. Gutacker, C.-Y. Lin, L. Ying, T.-Q. Nguyen, U. Scherf and G. C. Bazan, *Macromolecules*, 2012, **45**, 4441.
- 14 T. Ghooos, J. Brassinne, C.-A. Fustin, J.-F. Gohy, M. Defour, N. Van den Brande, B. Van Mele, L. Lutsen, D. J. Vanderzande and W. Maes, *Polymer*, 2013, **54**, 6293.
- 15 (a) R. D. McCullough, *Adv. Mater.*, 1998, **10**, 93; (b) K. Faied, M. Frechette, M. Ranger, L. Mazerolle, I. Levesque, M. Leclerc, T.-A. Chen and R. D. Rieke, *Chem. Mater.*, 1995, **7**, 1390.
- 16 M. T. Dang, L. Hirsch, G. Wantz and J. D. Wuest, *Chem. Rev.*, 2013, **113**, 3734.
- 17 (a) K. Yao, L. Chen, Y. Chen, F. Li and P. Wang, *J. Mater. Chem.*, 2011, **21**, 13780; (b) J. H. Seo, A. Gutacker, Y. Sun, H. Wu, F. Huang, Y. Cao, U. Scherf, A. J. Heeger and G. C. Bazan, *J. Am. Chem. Soc.*, 2011, **133**, 8416; (c) Y.-M. Chang, R. Zhu, E. Richard, C.-C. Chen, G. Li and Y. Yang, *Adv. Funct. Mater.*, 2012, **22**, 3284.
- 18 (a) J. Kesters, T. Ghooos, H. Penxten, J. Drijkoningen, T. Vangerven, D. M. Lyons, B. Verreet, T. Aernouts, L. Lutsen, D. Vanderzande, J. Manca and W. Maes, *Adv. Energy Mater.*, 2013, **3**, 1180; (b) S. Khiev, L. Derue, G. Ayenew, H. Medlej, R. Brown, L. Rubatat, R. C. Hiorns, G. Wantz and C. Dagron-Lartigau, *Polym. Chem.*, 2013, **4**, 4145.
- 19 (a) I. Osaka and R. D. McCullough, *Acc. Chem. Res.*, 2008, **41**, 1202; (b) K. Okamoto and C. K. Luscombe, *Polym. Chem.*, 2011, **2**, 2424; (c) A. Kiriy, V. Senkovskyy and M. Sommer, *Macromol. Rapid Commun.*, 2011, **32**, 1503.
- 20 (a) A. E. Javier, S. R. Varshney and R. D. McCullough, *Macromolecules*, 2010, **43**, 3233; (b) A. Sui, X. Shi, S. Wu, H. Tian, Y. Geng and F. Wang, *Macromolecules*, 2012, **45**, 5436.
- 21 M. C. Stefan, A. E. Javier, I. Osaka and R. D. McCullough, *Macromolecules*, 2008, **42**, 30.
- 22 M. A. Green, K. Emery, Y. Hishikawa and W. Warta, *Progress in Photovoltaics: Research and Applications*, 2009, **17**, 85.
- 23 (a) S. Clément, F. Meyer, J. De Winter, O. Coulembier, C. M. L. Vande Velde, M. Zeller, P. Gerbaux, J.-Y. Balandier, S. Sergeev, R. Lazzaroni, Y. Geerts and P. Dubois, *J. Org. Chem.*, 2010, **75**, 1561; (b) M. C. Stefan, M. P. Bhatt, P. Sista and H. D. Magurudeniya, *Polym. Chem.*, 2012, **3**, 1693; (c) R. J. Ono, S. Kang and C. W. Bielawski, *Macromolecules*, 2012, **45**, 2321; (d) Y.-H. Lin, K. A. Smith, C. N. Kempf and R. Verduzco, *Polym. Chem.*, 2013, **4**, 229.
- 24 S. Clément, A. Tizit, S. Desbief, A. Mehdi, J. De Winter, P. Gerbaux, R. Lazzaroni and B. Boury, *J. Mater. Chem.*, 2011, **21**, 2733.
- 25 J. De Winter, G. Deshayes, F. Boon, O. Coulembier, P. Dubois and P. Gerbaux, *J. Mass Spectrom.*, 2011, **46**, 237.
- 26 R. L. Danley, P. A. Caulfield and S. R. Aubuchon, *Am. Lab.*, 2008, **40**, 9.
- 27 S. Wouters, F. Demir, L. Beenaerts and G. Van Assche, *Thermochim. Acta*, 2012, **530**, 64.
- 28 P. G. Seybold and M. Gouterman, *J. Mol. Spectrosc.*, 1969, **31**, 1.
- 29 International Organisation for Standardisation (ISO), *International Standard ISO22412 Particle Size Analysis – Dynamic Light Scattering*, 2008.
- 30 R. K. Heenan, S. E. Rogers, D. Turner, A. E. Terry, J. Treadgold and S. M. King, *Neutron News*, 2011, **22**, 19.
- 31 <http://www.mantidproject.org>.
- 32 G. D. Wignall and F. S. Bates, *J. Appl. Crystallogr.*, 1987, **20**, 28.
- 33 I. Livsey, *J. Chem. Soc., Faraday Trans. 2*, 1987, **83**, 1445.
- 34 (a) L. Zhai, R. L. Pilston, K. L. Zaiger, K. K. Stokes and R. D. McCullough, *Macromolecules*, 2003, **36**, 61; (b) S. Miyanishi, K. Tajima and K. Hashimoto, *Macromolecules*, 2009, **42**, 1610.
- 35 R. Miyakoshi, A. Yokoyama and T. Yokozawa, *Macromol. Rapid Commun.*, 2004, **25**, 1663.
- 36 J. Liu, R. S. Loewe and R. D. McCullough, *Macromolecules*, 1999, **32**, 5777.
- 37 R. Puffr and J. Šebenda, *J. Polym. Sci.*, 1967, **16**, 79.
- 38 (a) R. D. McCullough, S. Tristram-Nagle, S. P. Williams, R. D. Lowe and M. Jayaraman, *J. Am. Chem. Soc.*, 1993, **115**, 4910; (b) W. D. Oosterbaan, V. Vrindts, S. Berson, S. Guillerez, O. Douhéret, B. Ruttens, J. D'Haen, P. Adriaensens, J. Manca, L. Lutsen and D. Vanderzande, *J. Mater. Chem.*, 2009, **19**, 5424.
- 39 M. Sundberg, O. Inganäs, S. Stafström, G. Gustafsson and B. Sjögren, *Solid State Commun.*, 1989, **71**, 435.
- 40 (a) C. Tan, M. R. Pinto and K. S. Schanze, *Chem. Commun.*, 2002, 446; (b) S. Wang and G. C. Bazan, *Chem. Commun.*, 2004, 2508; (c) H. D. Burrows, S. M. Fonseca, C. L. Silva, A. A. C. C. Pais, M. J. Tapia, S. Pradhan and U. Scherf, *Phys. Chem. Chem. Phys.*, 2008, **10**, 4420.
- 41 P. W. Schmidt, Some Fundamental Concepts and Techniques Useful in Small-Angle Scattering Studies of Disordered Solids, in *Modern Aspects of Small-Angle Scattering*, ed. H. Brumberger, Kluwer Academic Publishers, Dordrecht, The Netherlands, 1995, pp. 1–56.
- 42 *CRC Handbook of Chemistry and Physics*, ed. D. W. H. Rankin, Taylor & Francis, New York, 2009.